IJICTR
International Journal of Information & Communication Technology Research

Volume 11- Number 2 – Spring 2019 (7 -17)

Downloaded from journal.itrc.ac.ir at 11:54 IRDT on Wednesday August 26th 2020

A 3D Time-Variant Non-Stationary Hybrid Channel Model for Massive MIMO Systems

Mohammad Mehdi Tamaddondar
Department of Communication Technologies
ICT Research Institute,
Tehran, Iran
tamaddondar@itrc.ac.ir

Narges Noori*
Department of Communication Technologies
ICT Research Institute,
Tehran, Iran
nnoori@itrc.ac.ir

Received: 22 August 2018 - Accepted: 21 March 2019

Abstract—**This paper presents a novel three-dimensional (3D) time-variant hybrid channel model for massive multiple input multiple output (M-MIMO) wireless systems. The main aim of the proposed model is to find channel characteristics in a simple and precise manner. To achieve this purpose, this channel model consists of two deterministic and stochastic modes. By using the idea of equivalent planes and ray tracing method, the channel multipath components (MPCs) are calculated in the deterministic mode. In the stochastic mode, those parts of the propagation environment that are too complex to be modeled in the deterministic mode, are modeled based on the cluster concept. Then, the MPCs characteristics are calculated by utilizing appropriate random distributions. The doppler effect is also taken into account due to the probability of existence relative velocities among channel components. This model is validated by comparing simulation results with those of the previously developed channel models. Finally, the channel model is applied to a real scenario to extract some of the important characteristics of the propagation environment.**

Keywords-Channel modeling, doppler effect, clustering, massive MIMO, ray tracing, 5G

I. INTRODUCTION

The fifth generation (5G) of mobile communication systems is expected to significantly enhance characteristics of the wireless networks. Three main improvements in 5G are: (i) enhanced mobile broadband, (ii) massive machine type communications and (iii) ultra-reliable and low latency communications [1, 2]. Furthermore, 5G wireless systems are aimed to be adapted with a wide range of indoor, urban, suburban and rural propagation environment [3, 4]. Massive multiple input multiple output (M-MIMO) is a promising key candidate technology for 5G deployment [5-9]. A M-MIMO system is equipped with tens or hundreds of antenna elements at the base station (BS) to simultaneously serve tens of users. These huge numbers of antenna elements help M-MIMO systems have steerable beams and improve their spectral and energy efficiencies as well as their capacity and reliability. This allows a higher number of user equipment (UE) connections with respect to the conventional MIMO systems [1, 3, 9-14].

An important issue in M-MIMO wireless communications is to properly allocate channel link budget. Accordingly, channel modeling is an essential step in a M-MIMO system design. Measurement results show that several new characteristics such as non-

* Corresponding Author

www.SID.ir

Downloaded from journal.itrc.ac.ir at 11:54 IRDT on Wednesday August 26th 2020

stationary channel properties and spherical wave (SW) fronts need to be considered in the M-MIMO arrays which makes them significantly different from the conventional MIMO systems [3, 15, 16]. Many channel modeling efforts have been performed to extract different characteristics of the M-MIMO propagation channels. These models have been generally based on some theoretical analysis or measurement for different scenarios. The non-stationary and birth-death properties of the channel are considered in [9, 17]. A twin multi-ring channel model is presented in [18] to investigate SW assumption in M-MIMO systems. This model also considers appearance and disappearance of the clusters on both array and time axes. Some of the other channel models are map-based. In [19], a channel model is proposed based on the map of propagation environment where the ray tracing algorithm is utilized to calculate channel characteristics. The 3D theoretical channel models of [20] and [21] have been developed to investigate non-stationary properties and some other channel features based on the cluster-level evolution process in both space and time domains. The non-stationary birth-death (BD) process in time and array domains is considered in [22] for 3D channel where the base station (BS) is equipped with a uniform planar antenna array. A 3D geometric-based stochastic channel model (GBSM) is proposed in [23] which includes non-stationary properties of the channel based on WINNER II [24] and Saleh-Valenzuela (SV) [25] channel models. Measurement-based channel models provide an effective way to study behavior of the M-MIMO channels [26]. These channel models help the researchers observe theoretical hypotheses i.e. the appearance and disappearance of the clusters on the array axis. Different algorithms such as K-mean are used for post-processing of the measured data. In [27], the authors have utilized space-alternating generalized expectation maximization (SAGE) and K-mean algorithm for estimation, tracking and clustering the MPCs.

Recently, M-MIMO based 5G vehicular communications have attracted extensive attractions [28-30]. In vehicular communications, some specific phenomena such as the doppler shift (DS) occurs due to the relative velocity of the transmitter (Tx), receiver (Rx) and interacting objects (IOs). In [31, 32], a geometry-based channel model has been presented for vehicular communication where the channel non-stationary phenomenon is investigated through autocorrelation function (ACF) of channel impulse response (CIR). The authors in [33] proposed a 3D non-stationary vehicle-to-vehicle (V2V) channel model and considered SW property as well as DS. A two-ring mobile-to-mobile channel model is presented in [34, 35] where different propagation phenomena including line-of-sight (LoS), single-bounce (SB) and double-bounce (DB) conditions are considered to investigate doppler power spectrum of these channels at millimeter wave frequencies. Some of these measurement-based channel models with their overall properties are summarized in Tab. 1.

In this paper, we propose a 3D hybrid model for time-variant non-stationary M-MIMO channels. This model consists of two deterministic and stochastic modes. In the deterministic mode, those parts of the propagation environment that can be mapped to some surfaces such as walls, floor and ramps are defined as ideal planes with defined boundaries. Then, the ray tracing algorithm is applied to model all reflection and transmission paths created by these surfaces between the BS antenna elements and mobile stations (MSs). The stochastic mode considers those parts of the propagation environment that are too complex to be modeled in the deterministic mode. This mode is based on the cluster concept [27, 36-37]. After mapping the channel to the appropriate clusters, K-mean algorithm is used to update cluster locations in each snapshot. Then, appropriate random distributions are applied to extract characteristics of the channel by considering DS of the MPCs in each cluster. Finally, both deterministic and stochastic modes are integrated to extract channel characteristics including CIR, power delay profile (PDP), power angular profile (PAP) and angle of arrivals (AoAs). The distinctive advantages of the proposed channel model are its simple and fast implementation even for complex environments. Furthermore, the model has high accuracy since it is based on the real channel geometry. To evaluate the proposed method, simulation results are compared with those reported in [31]. The channel model is also applied to a real scenario to extract characteristics of the propagation environment.

Tab. 1. Measurement based channel models and their features.

Ref.	Features			
	f [GHz]	Antenna Topology	Scenario	Observations
[38]	2/4/6	64-vitual LA	Indoor	Path loss, PDP, Root Mean Square (RMS) delays spread.
[39]	2.6	128-virtual LA	Outdoor	Non-Stationary, Channel Gain, Angular power Spread (APS).
[40]	3.3	64-LA & PA	Outdoor	Non-stationary, PDP, PAS, DS, Angular Spread (AS).
[41]	5.8	64-LA & PA	Indoor	Non-Stationary, Channel Orthogonality, Power variation along the array.
[27]	6	256-virtual URA	Indoor	Intra-cluster parameters, (AS), Existence of Clusters and MPCs along the array axis.
[42]	11	256-virtual URA	Indoor	Non-stationary in elevation and azimuth directions, SW assumption.
[43]	11/16/28/38	51 /76 /91/121-PA	Indoor	Non-Stationary, PDP, PAP, RMS DS.
[44]	13~17	400-PA	Indoor	Channel Gain, RMS DS.
[45]	15	1600-Virtual PA	Outdoor	Non-Stationary, AoA, Number of clusters, DS.
[26]	26	64 &128-vitual LA & PA	Indoor	PDP, RMS delay, Coherence Bandwidth.

www.SID.ir

Downloaded from journal.itrc.ac.ir at 11:54 IRDT on Wednesday August 26th 2020

The contributions of this paper are summarized as follows:

- A novel 3D channel model is proposed in this paper for simple extraction of the M-MIMO channel characteristics.
- The spatial non-stationary property of the M-MIMO channels is considered along the array axis.
- The doppler frequency is taken into account for time-variant channels where channel components may have relative velocity.
- The graphical interface between real propagation environment and the simulator has been constructed through equivalent planes and spheres in the deterministic and stochastic modes, respectively. This idea can simply increases correlation between the real channel and simulations.
- Different antenna characteristics such as radiation pattern, polarization and mismatch coefficient can be imported in the simulator to make the more precise channel modeling.

In the rest of the paper, the abbreviations and terms presented in Tab. 2 will be used.

Tab. 2. A list of abbreviations and terms used in the paper.

3D	Three dimensional
5G	Fifth Generation
ACF	Auto Correlation Function
AoA	Angle of Arrival
AoD	Angle of Departure
APS	Angular Power Spread
AS	Angular Spread
BD	Birth Death
BS	Base Station
CCF	Cross Correlation Function
CIR	Channel Impulse Response
Cx	Cluster
DR	Double Reflection
DB	Double Bounce
DS	Delay Spread
EM	Electromagnetic
GBSM	Geometric Based Stochastic Model
IO	Interacting Object
LoS	Line of Sight
M-MIMO	Massive Multiple Input Multiple Output
MPC	Multipath Component
MS	Mobile Station
PAP	Power Angular Profile
PDP	Power Delay Profile
Rx	Receiver
RC	Range Cell
RMS	Root Mean Square
SAGE	Space Alternating Generalized Expectation maximization
SB	Single Bounce
SR	Single Reflection
SV	Saleh Valenzuela
SW	Spherical Wave
Tx	Transmitter
UE	User Equipment
V2V	Vehicular to Vehicular
WINNER	Wireless World Initiative New Radio

II. Time-Variant Non Stationary Channel Modeling Algorithm

The first step of the channel modeling framework is to define channel structure as shown in Fig. 1. This includes positions of the BS antenna elements and MSs as well as their 3D configurations in each snapshot. Since both BS and MS may have motion in the direction of their velocity vectors, their locations are updated in each snapshot. Different kinds of IOs may exist in the channel, which are modeled in deterministic or statistic modes according to their structures.

A. Deterministic Mode

In the deterministic mode, those IOs that are in the form of surfaces such as walls, floors, ceilings and ramps are mapped to the rectangular planes. These planes are defined by their corners. The LoS and reflection paths between the BS antenna elements and all MSs are calculated in this mode. Both single reflection (SR) and double-reflection (DR) paths are calculated by applying image theory. If there is any plane in the trajectory of the ray, its transmission coefficient is considered to calculate the received signal at the MS. The LoS, SR, and DR components are all shown in Fig. 1. All parameters used in Fig.1 are listed and defined in Tab. 3.

B. Stochastic Mode

According to Fig. 1, those parts of the propagation environment that cannot be modeled deterministically due to their complex geometric structure are considered in the stochastic mode. The stochastic mode is based on the cluster concept. The rays that reach the MS with similar delays and AoAs, are formed a cluster. In order to define clusters, some spheres with different radii are assumed. The centers of all spheres are located in the MS position.

Tab. 3. Definitions of geometry parameters

$\mathbf{v}_m^{Tx}$	velocity vector of the *m*th element at Tx side
$\mathbf{v}_n^{Rx}$	velocity vector of the *n*th element at Rx side
$\mathbf{v}_q^{Cx}$	velocity vector of the *q*th cluster
$\mathbf{D}_{m,n}^{LoS}$	LoS vector between the *m*th and the *n*th elements at Tx and user, respectively
$\mathbf{D}_{m,R1}^{SR}$	single reflection vector between the *m*th antenna at Tx and reflection point *R1*
$\mathbf{D}_{R1,n}^{SR}$	single reflection vector between the *n*th user and reflection point *R1*
$\mathbf{D}_{m,R1}^{DR}$	double reflection vector between the *m*th antenna at Tx and reflection point *R1*
$\mathbf{D}_{R2,n}^{DR}$	double reflection vector between the *n*th user and reflection point *R2*
$\mathbf{D}_{m,Cxq}^{SB}$	single bounce vector between the *m*th antenna at *Cxq*
$\mathbf{D}_{Cxq,n}^{SB}$	single bounce vector between *Cxq* the *n*th user
$\mathbf{D}_{m,Cx1,l}^{DB}$	double bounce vector between the *m*th antenna at Tx and *Cx1* in *l*th double bounce
$\mathbf{D}_{Cx1,Cx2,l}^{DB}$	double bounce vector between *Cx1 and Cx2* in the *l*th double bounce
$\mathbf{D}_{Cx2,n,l}^{DB}$	double bounce vector between *Cx2* and the *n*th user in *l*th double bounce

www.SID.ir

Downloaded from journal.itrc.ac.ir at 11:54 IRDT on Wednesday August 26th 2020

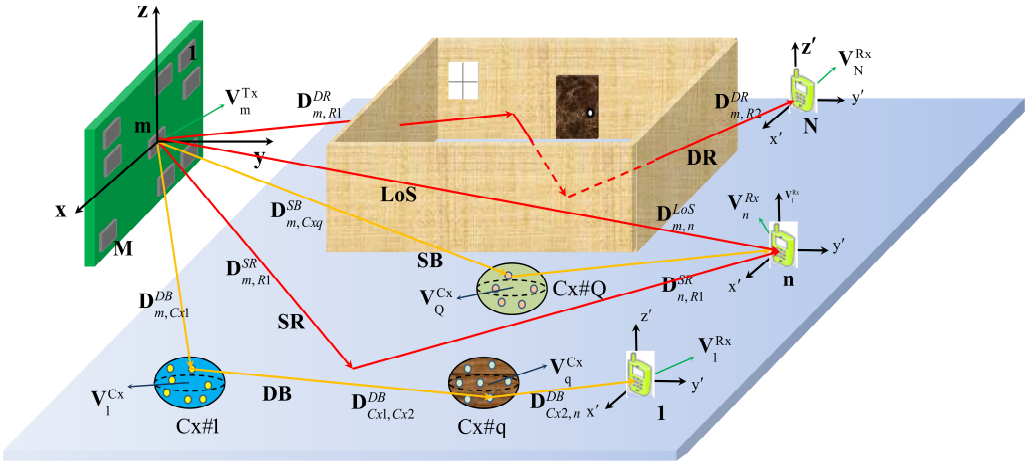

Fig. 1. An overview of a typical M-MIMO channel in one snapshot.

Those parts of the propagation environment which defined in the stochastic mode, are mapped with corresponding clusters. To this end, spheres with additive radii, r_i, are considered around the MS. The spheres are expanded to cover the entire space surrounded by the environment boundaries. Their radii are defined as follows depending on the amount of the delay intended to distinguish the distinct clusters, $\Delta\tau$:

$$r_i = ic_o\Delta\tau \qquad (1)$$

where c_0 is the speed of light and $i = 0,1,2,...,N_i$. The number of spheres denotes by N_i. Then, each sphere is divided into equal angular spaces in both elevation and azimuth directions. Based on the cluster AoAs definition, the angular limitation in the azimuth and elevation directions are $\Delta\varphi$ and $\Delta\theta$, respectively. The space between each two adjacent spheres, which is limited with angular space in both elevation and azimuth directions, is defined as a 3D range cell (RC) as shown in Fig. 2.

In our simulations, the cluster delay is set to 5 ns and cluster AoAs in both the azimuth and elevation directions are considered to be 15 degrees. The azimuth cross section of a RC containing some IOs and the corresponding cluster-assignments are illustrated in Fig. 3. a and Fig. 3. b, respectively. We apply K-mean algorithm to assign the best cell to the adjacent IOs. If there is an IO in a RC, that RC can make one signal path to the MS. This makes single-bounce (SB) paths between the BS and MS. The same sphere can also be considered around the BS location. In the double-bounce (DB) case, the rays first hit to the IOs in the RCs at the BS side, then reach to the IOs in the RCs at the MS side, and finally reach the MS. When a ray hit a cluster and exit it, different phenomena may occur within the cluster. Hence, several orders of reflection and transmissions are considered to model these phenomena. There is also intra-cluster delay inside each cluster, which is considered to calculate overall delay. Fig.4 shows the mentioned intra-cluster phenomena.

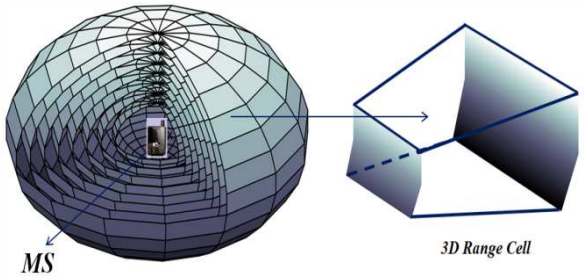

Fig. 2. 3D range cells around a MS.

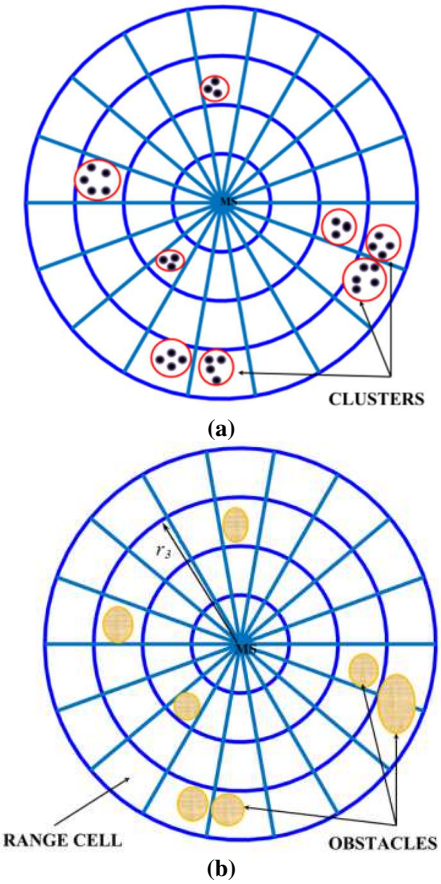

Fig. 3. Azimuth cross section of a RC a) initial obstacles, b) corresponding clusters.

www.SID.ir

Downloaded from journal.itrc.ac.ir at 11:54 IRDT on Wednesday August 26th 2020

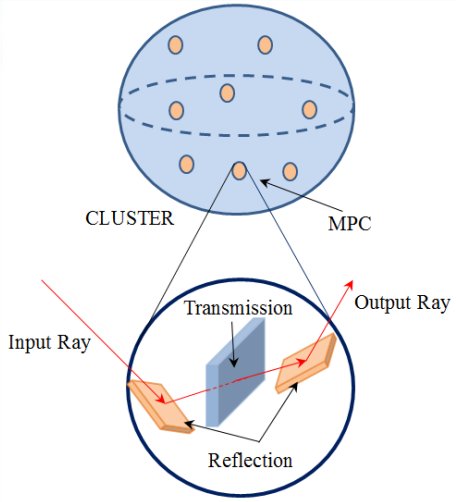

Fig. 4. Intra-cluster reflection and transmission phenomena.

Tab. 4. Random distributions for channel variables.

Variable	Proposed Distribution
Phase Shift of MPCs	Uniform [46]
Number of MPCs	Poisson [47]
Time Delay of MPC	Exponential [46]
AoA & AoD	Guassian or Von Mises [21, 48]

In each snapshot, the positions of BS, MSs and IOs are updated according to their velocity vectors. Appropriate random distributions, presented in Tab. 4, are applied to extract characteristics of the channel stochastic parts including signal strength, delays, phase shifts and AoAs. The channel modeling algorithm is summarized in the flowchart of Fig. 5.

III. Detail Mathematic Of Channel Modeling

Some deterministic and stochastic mathematical relations are utilized to extract channel characteristics of the M-MIMO systems. The channel matrix of a M-MIMO system equipped with M antenna element at the BS serves N single antenna MSs can be presented by a $M \times N$ complex time-variant matrix $\mathbf{H}(t,\tau) = \left[h_{m,n}(t,\tau)\right]_{M\times N}$ where $m = 1,2,\cdots,M$, $n = 1,2,\cdots,N$ and $h_{m,n}(t,\tau)$ is the multipath gain from the mth BS antenna to the nth MS and is expressed as follows:

$$h_{m,n}^{T} = h_{m,n}^{d} + h_{m,n}^{s} \tag{2}$$

where $h_{m,n}^{d}$ and $h_{m,n}^{s}$ are the multipath gains in the deterministic and stochastic modes, respectively.

A. Mathematics of deterministic channel modeling

First, in the deterministic mode, image theory is applied to find propagation paths between the mth BS antenna and the nth user. Deterministic CIR between the mth BS antenna and the nth user, $h_{m,n}^{d}$, consists of LoS, SR and DR components:

$$h_{m,n}^{d} = h_{m,n}^{LoS} + h_{m,n}^{SR} + h_{m,n}^{DR} \tag{3}$$

The LoS component of (3) is given by:

$$h_{m,n}^{LoS}(t,\tau) = \frac{\prod_{u=1}^{U_T^{LoS}} T_u^{LoS}}{4\pi r_{m,n}} \lambda_c \cdot \exp(-i2\pi(f_c + f_D^d)\tau) \times g_m^{Tx}(\theta^{Tx},\varphi^{Tx}) \cdot g_n^{Rx}(\theta^{Rx},\varphi^{Rx}) \tag{4}$$

where $u = \{1,2,...,U_T^{LoS}\}$ is the number of surfaces that the LoS component passes and T_u^{LoS} is transmission coefficient of the uth surface. The AoD in both elevation and azimuth planes are θ^{Tx} and φ^{Tx}, respectively, while g_m^{Tx} is the mth BS antenna gain. The AoA in both elevation and azimuth planes for the LoS ray are θ^{Rx} and φ^{Rx}, respectively, while g_n^{Rx} is the n th user's antenna gain. The wavelength of the carrier frequency, f_c, is denoted by λ_c and the doppler frequency in deterministic mode is f_D^d. The SR component is given by:

$$h_{m,n}^{SR}(t,\tau) = \sum_{k=1}^{K_{SR}} R_k^{SR} \frac{\prod_{u=1}^{U_k^{SR}} T_{u,k}^{SR}}{4\pi r_k} \lambda_c \cdot \exp(-i2\pi(f_c + f_D^d)\tau_k) \times g_m^{Tx}(\theta_k^{Tx},\varphi_k^{Tx}) \cdot g_n^{Rx}(\theta_k^{Rx},\varphi_k^{Rx}) \tag{5}$$

where subscript k denotes to the k th path. The number of SRs between the mth BS antenna and the n th user is K_{SR} and the reflection coefficient in the k th path is R_k^{SR}. The number of transmission in the k th path is shown by U_k^{SR} and the u th transmission coefficient in the k th path is $T_{u,k}^{SR}$. The DR component is given by:

$$h_{m,n}^{DR}(t,\tau) = \sum_{k=1}^{K_{DR}} R_{1,k}^{DR} R_{2,k}^{DR} \frac{\prod_{u=1}^{U_k^{DR}} T_{u,k}^{DR}}{4\pi r_k} \lambda_c \cdot \exp(-i2\pi(f_c + f_D^d)\tau_k) \times g_m^{Tx}(\theta_k^{Tx},\varphi_k^{Tx}) \cdot g_n^{Rx}(\theta_k^{Rx},\varphi_k^{Rx}) \tag{6}$$

where the number of DR components is K_{DR}. As mentioned before, the DR components experience two reflections in the kth path between the mth BS antenna and the nth user, where their corresponding reflection coefficient are shown by $R_{1,k}^{DR}$ and $R_{2,k}^{DR}$. The DR components may face several transmissions along their paths where total number of transmissions and their corresponding coefficients in the kth path are U_k^{DR} and $T_{u,k}^{DR}$, respectively.

www.SID.ir

Downloaded from journal.itrc.ac.ir at 11:54 IRDT on Wednesday August 26th 2020

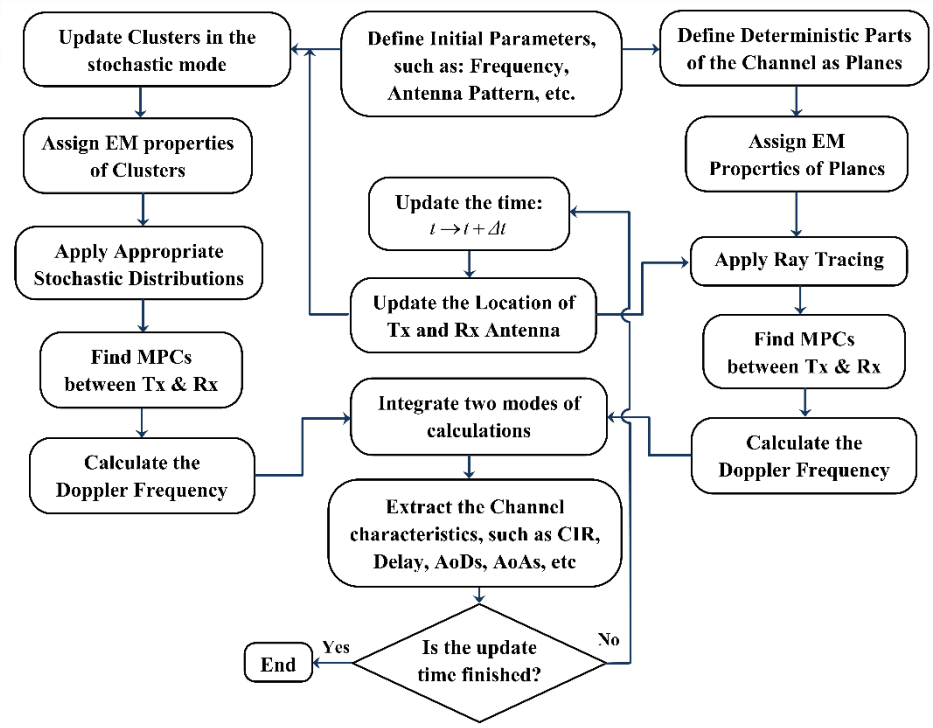

Fig. 5. Flowchart of the channel modeling algorithm.

B. Mathematics of stochastic channel modeling

As mentioned in the previous section, those parts of the channel that due to their complexity cannot be modeled in the deterministic mode are mapped to some clusters. As shown in Fig. 4, by considering both SB and DB paths with intra-cluster reflection and transmission phenomena, the stochastic CIR, $h_{m,n}^{s}$, can be written as:

$$h_{m,n}^{s} = h_{m,n}^{SB} + h_{m,n}^{DB} \tag{7}$$

where the superscript *s* denotes to the stochastic mode. The SB channel gain $h_{m,n}^{SB}$ is given by:

$$h_{m,n}^{SB}(t,\tau) = \sum_{q=1}^{Q^{SB}} \sum_{k=1}^{K_q^{SB}} \frac{\prod_{u=1}^{U_k^{SB}} R_{u,k}^{SB} \prod_{w=1}^{W_k^{SB}} T_{w,k}^{SB}}{4\pi r_{q,k}} \times \lambda_c \cdot \exp(-i2\pi(f_c + f_{D,qk}^{SB})\tau_{q,k}^{SB}) \cdot \exp(-i\varphi_{q,k}^{SB}) \times g_m^{Tx}(\theta_{q,k}^{Tx}, \varphi_{q,k}^{Tx}) \cdot g_n^{Rx}(\theta_{q,k}^{Rx}, \varphi_{q,k}^{Rx}) \tag{8}$$

$$\tau_{q,k}^{SB} = \tau_{q,k} + \tau_q^{SB} \tag{9}$$

$$\tau_{q,k} = \frac{r_{q,k}}{c_0} \tag{10}$$

where $\tau_{q,k}^{SB}$ is overall time delay corresponding to the k th path through the q th cluster and τ_q^{SB} denotes the intra-cluster time delay of the q th cluster in the SB component. In (10), $r_{q,k}$ is total length of the k th path through the q th cluster and $\tau_{q,k}^{SB}$ is its corresponding delay. The doppler frequency is denoted by $f_{D,q,k}^{SB}$. Other parameters of the stochastic mode are listed in Tab. 5.

Tab. 5. Parameters of stochastic channel modeling.

Q^{SB}	Total number of clusters around MS
K_q^{SB}	Number of MPCs within the *q*th cluster
U_q^{SB}	Number of reflection within the *k*th MPC
W_k^{SB}	Number of transmission within the *k*th MPC
$\varphi_{q,k}^{SB}$	SB phase shift of the *k*th path in the the *q*th cluster
τ_q^{SB}	Intra-cluster delay of the *q*th cluster in the SB component
L^{DB}	Number of DB components equals to $L^{DB} = \min\{ Q_{MS}^{DB}, Q_{BS}^{DB} \}$
Q_{BS}^{DB}	Number of clusters around BS in DB mode
Q_{MS}^{DB}	Number of clusters around MS in DB mode
K_l^{DB}	Number of MPCs within the *l*th DB component
U_k^{Cx1}	Number of reflection within the *k*th path in the first cluster of the *l*th DB component
W_k^{Cx1}	Number of transmission within the *k*th path in the first cluster of the *l*th DB component
U_k^{Cx2}	Number of reflection within the *k*th path in the second cluster of the *l*th DB component
W_k^{Cx2}	Number of transmission within the *k*th path in the second cluster of the *l*th DB component
$\varphi_{l,k}^{Cx1}$,	DB phase shift of the *k*th path in the the *l*th component within first cluster
$\varphi_{l,k}^{Cx2}$	The DB phase shift of the *k*th path in the the *l*th component within second cluster
τ_l^{DB}	Intra-cluster delay of the first and second clusters in the *l*th DB component

www.SID.ir

Downloaded from journal.itrc.ac.ir at 11:54 IRDT on Wednesday August 26th 2020

The AoD and AoA in the azimuth and elevation planes of the k th path in the q th case are $(\theta_{q,k}^{Tx}, \varphi_{q,k}^{Tx})$ and $(\theta_{q,k}^{Rx}, \varphi_{q,k}^{Rx})$, respectively. The DB channel gain $h_{m,n}^{DB}$ is given by:

$$h_{m,n}^{DB}(t,\tau) = \sum_{l=1}^{L^{DB}} \sum_{k=1}^{K_l^{DB}} \frac{\prod_{u1=1}^{U_{l,k}^{Cx1}} \prod_{w1=1}^{W_{l,k}^{Cx1}} \prod_{u2=1}^{U_{l,k}^{Cx2}} \prod_{w2=1}^{W_{l,k}^{Cx2}} R_{u1,l,k}^{Cx1} T_{w1,l,k}^{Cx1} R_{u2,l,k}^{Cx2} T_{w2,l,k}^{Cx2}}{4\pi r_{l,k}}$$
$$\times \lambda_c \cdot \exp(-i2\pi(f_c + f_{D,l,k}^{DB})\tau_{l,k}^{DB}) \cdot \exp(-i(\varphi_{l,k}^{Cx1} + \varphi_{l,k}^{Cx2}))$$
$$\times g_m^{Tx}(\theta_{l,k}^{Tx}, \varphi_{l,k}^{Tx}) \cdot g_n^{Rx}(\theta_{l,k}^{Rx}, \varphi_{l,k}^{Rx}) \quad (11)$$

IV. Modeling Scenario And Simulation Results

The channel modeling algorithm is implemented in MATLAB software. Two different scenarios are considered. In the first scenario, we model an indoor channel that has been previously investigated in [36] by performing some measurement. In the second scenario, we verify performance of our simulator by comparing the results with those of the one-ring channel model [31].

A. Validation scenario

In order to validate channel modeling algorithm, we consider two different propagation environments previously investigated by the measurements and one-ring model. The first environment is a Center Hall of a university where a measurement-based model has been developed. We model the outer walls of the propagation environment and both BS and MS locations in the simulator as shown in Fig. 6. Then, the ray tracing algorithm is applied to find the MPCs between the BS and MS. The seats are modeled in the stochastic mode by assigning appropriate clusters. Then, the MPCs in the stochastic mode are found by using random distributions as mentioned in Tab. 4. The operating frequency is set to 26 GHz. The BS is equipped with 64 linear antenna elements. The distance between the BS and the MS is about 4 m. The PDP of the channel between the first antenna element at the BS and the MS is computed and compared with the measurement result reported in [36], as depicted in Fig. 7. The simulation results show a high degree of agreement between the proposed channel model and the measurement.

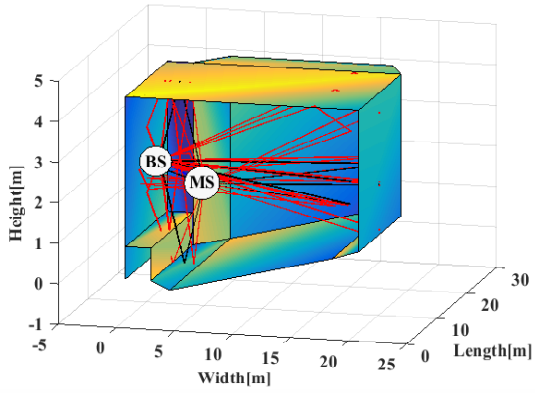

Fig. 6. A Center Hall of a university considered to verify the channel model.

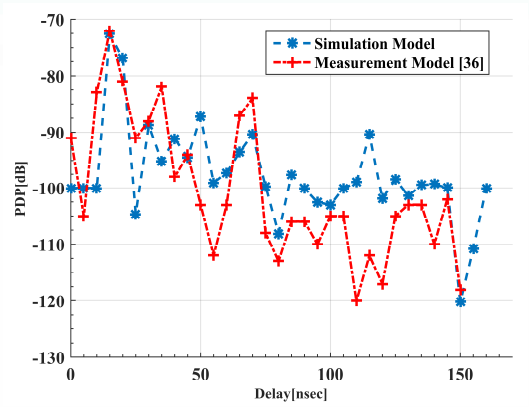

Fig. 7. Comparison between the results of proposed channel model and measurements reported in [36].

The second channel is an environment previously investigated by the one-ring channel model in [31]. As shown in Fig. 8, in this scenario, the user antenna is located at the origin of the coordination system and it is surrounded by N_c=20 clusters located in a ring with a radius of R=200 m. The user speed is $v_R = 110km/h$ along the vector $\mathbf{v}_R = [\cos(60), \sin(60), \ 0]$. The BS is located at a point with coordinates, $(-2000,0,0)$, while its speed is $v_T = 120km/h$ in the direction of $\mathbf{v}_T = [\cos(30), \sin(30), 0]$. The operating frequency is set to 26 GHz, and the successive array element spaces are set to one half of the wavelength. Transmission power is set to 30 dBm. The maximum doppler frequency corresponding to the BS and user are $f_{T\max}^d = 100Hz$ and $f_{R\max}^d = 91Hz$, respectively. A top view configuration of the BS, MS and scatters (clusters) is shown in Fig. 8. Different points in the BS and MS sides show their locations in different snapshots.

The channel response is calculated by implementing this scenario. Absolute time-variant ACF of the CIR is depicted in Fig. 9. The LoS component is not considered in this scenario as it is neglected in one-ring channel model presented in [31].

The smooth variations along the time axis indicate the non-stationary property of the channel. The simulated ACF snapshots at t=0, 0.5 and 1 S, are compared with the corresponding diagram of the one-ring channel model in Fig. 10. It can be seen that our simulation results coincide with the results of one-ring channel model.

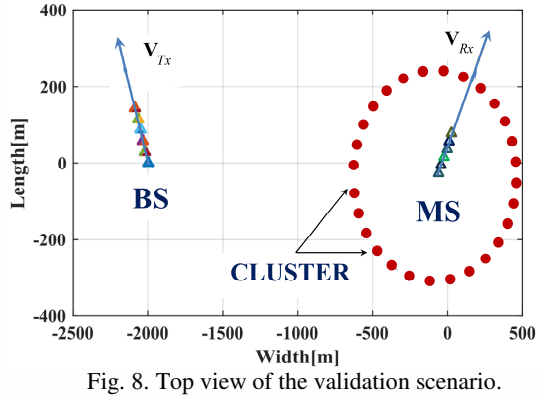

Fig. 8. Top view of the validation scenario.

www.SID.ir

Downloaded from journal.itrc.ac.ir at 11:54 IRDT on Wednesday August 26th 2020

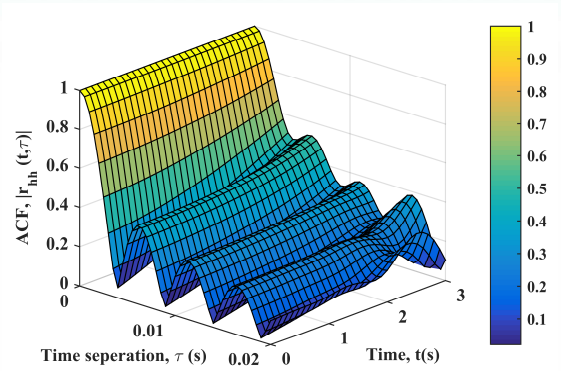

Fig. 9. Time-variant ACF of CIR obtained by the proposed channel model.

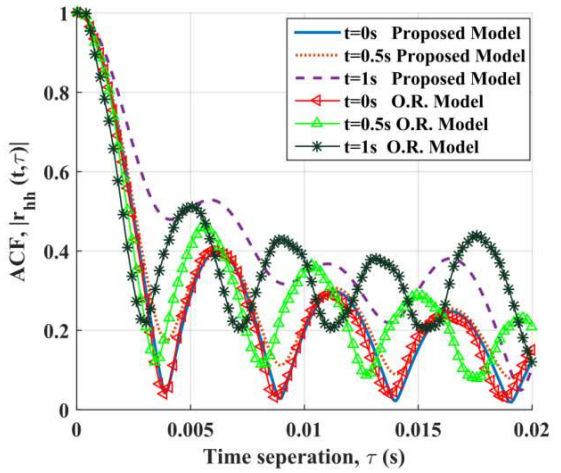

Fig. 10. Comparison between ACF of the CIR using the proposed channel model and one-ring channel model at different time snapshots.

The cross correlation function (CCF) is utilized to analyze distinct channels of different antenna elements. The space CCF of the proposed channel model against time and user distance, δ_R, is shown in Fig. 11. It can be seen that, by increasing distance between users, the correlation between two channels decreases with time.

Meanwhile, by increasing the distance between two adjacent antenna elements at the BS, δ_T, the correlation between two channels may not experience significant changes as depicted in Fig. 12.

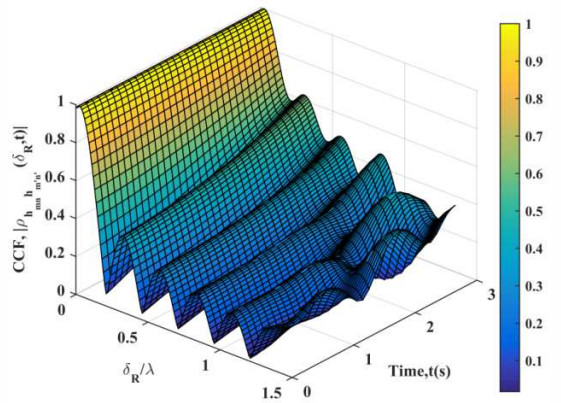

Fig. 11. Time-variant CCF of two distinct channels user distance.

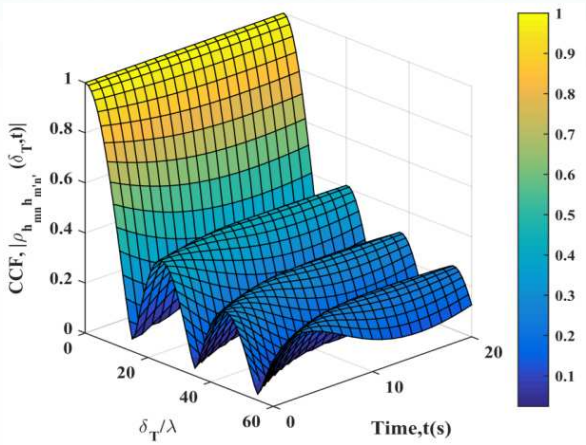

Fig. 12. Time-variant CCF of two distinct channels the antenna distance at BS.

B. Channel modeling of a real scenario

At the second step, the channel modeling algorithm is applied to a real 3D outdoor environment. In this scenario, the BS is equipped with 64 antenna elements in a linear configuration to cover 3 users. The details of the BS and MS antennas are given in Tab. 6. This environment includes several buildings, a green field area and a car parking. The buildings are modeled with equivalent planes, while the green area and car parking are modeled as clusters. Fig. 13 shows these IOs in the form of cubes and clusters.

The PDP of the channel between the first antenna element at BS side and the first user is shown in Fig. 14. Different MPCs can be distinguished in this figure. Fig. 15 shows the received power relative to AoA in both azimuth and elevation directions. Different clusters can be distinguished in Fig. 14 and Fig. 15 regarding to their similar delays and AoAs. In order to evaluate PDP changes along the array axis, the propagation channels between the first, 32*th* and the last antenna element of the BS and one MS are modeled and their corresponding PDPs are extracted. Figure 16 shows the PDP of these channels. Although the overall PDP are the same, some differences due to the non-stationary property can be observed between these different channels.

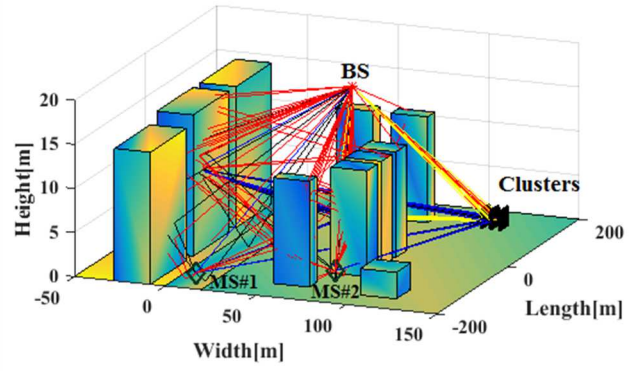

Fig. 13. 3D propagation scenario for channel modeling.

www.SID.ir

Downloaded from journal.itrc.ac.ir at 11:54 IRDT on Wednesday August 26th 2020

Tab. 6. Characteristics of the BS and MS.

	Center	Velocity Vector	No of Ant.	Config.	Pattern	Polarization
BS	[60,20.36,18]	[0,0,0]	64	Linear	Omnidirectional	Horizontal
MS#1	[13,-180,1.2]	[0,0,14]	single	-	Omnidirectional	Horizontal
MS#2	[80,-130,1.5]	[1.4,1.4,0]	single	-	Omnidirectional	Horizontal
MS#3	[12,-50,9]	[0,0,0]	single	-	Omnidirectional	Horizontal

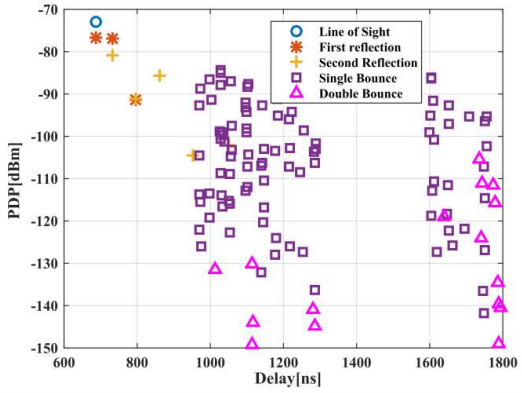

Fig. 14. PDP of the channel between the first antenna element of the BS and the first user.

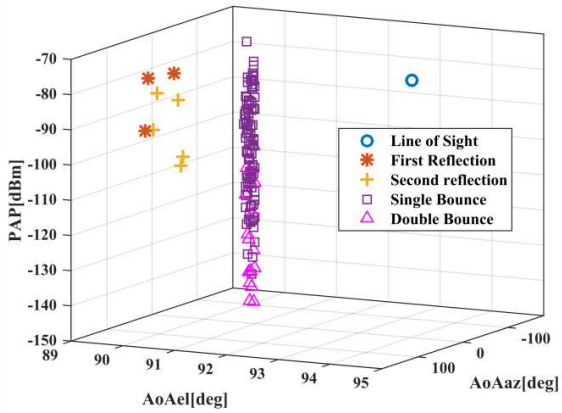

Fig. 15. PAP of the channel between the first antenna element of the BS and the first user relative to the azimuth and elevation angles.

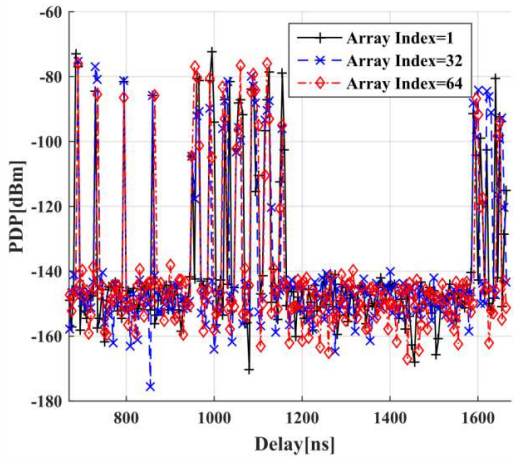

Fig. 16. PDP between three antenna elements at BS and first user.

The channel small scale and large scale fadings are shown in Fig. 17. Different MPCs arrive at the receiver with different phase shifts and therefore the received signals are either constructive or destructive.

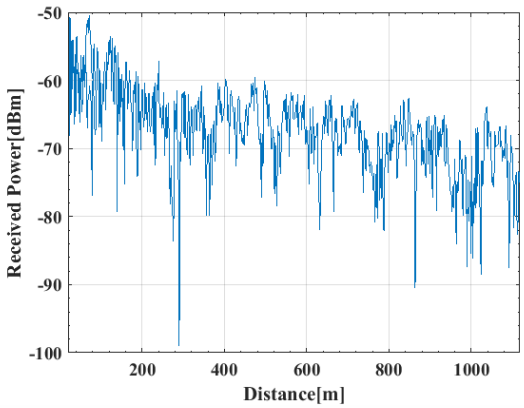

Fig. 17. Received power from the first antenna elements of the BS in the third user location versus distance.

V. CONCLUSION

A novel 3D time-variant hybrid channel model for M-MIMO systems is proposed in this paper which consists of two deterministic and stochastic modes. These modes help the simulation engine decrease complexity of the channel modeling without noticeable changes in the accuracy. Furthermore, this approach can significantly reduce modeling calculation time. The time-variance and non-stationary features of the channel are discussed and evaluated. The results of the proposed channel model are in high degree of agreement with those of the well-known one-ring channel model and measurements. Then, the proposed channel model is applied to a real propagation environment and channel characteristics such as PDP and PAP are extracted. The non-stationary features of the channel on both array and time axes can be observed in the simulation results.

REFERENCES

[1] T. Kashima, J., Qiu, H., Shen, et al. “Large scale massive MIMO field trial for 5G mobile communications system,” *International. Symposium on Antennas and Propagation. (ISAP),* pp. 602–603. Oct. 2016.

[2] G. A., Akpakwu, B. J., Silva, G. P., Hancke, et al. “A survey on 5G networks for the Internet of Things: Communication technologies and challenges,”. *IEEE Access,* vol. 6, pp. 3619–3647, Dec. 2018.

[3] C.-X., Wang, J., Bian, J., Sun, et al. “A Survey of 5G Channel Measurements and Models,” *IEEE Communications Surveys & Tutorials* , vol. 20, no. 4, pp. 3142–3168, Aug. 2018.

[4] C.-X., Wang, F., Haider, X., Gao, et al. “Cellular Architecture and Key Technologies for 5G Wireless Communication Networks,” *IEEE Communications Magazine,* , vol. 52, no. 2, pp. 122–130, Feb. 2014.

[5] O. I., Bismark, F., Idachaba,A., Atayero, “Massive MIMO Channel Characterization and Modeling: The Present and Future,” *International Journal of Applied Engineering Research*, vol. 12, no. 23, pp. 13742–13754, Dec. 2017.

[6] J. G., Andrews, S., Buzzi, W., Choi, et al. “What will 5G be?” *IEEE Journal on Selected Areas in Communications.,* vol. 32, no. 6, pp. 1065–1082, June 2014.

www.SID.ir

Downloaded from journal.itrc.ac.ir at 11:54 IRDT on Wednesday August 26th 2020

[7] J. O., Nielsen, W., Fan, P. C., Eggers, et al. "A Channel Sounder for Massive MIMO and MmWave Channels," *IEEE Communications Magazine*, vol. 56, no. 12, pp. 67–73, Dec. 2018.

[8] R., Zhang, Z., Zhong, J., Zhao, et al. "Channel Measurement and Packet-Level Modeling for V2I Spatial Multiplexing Uplinks Using Massive MIMO," *IEEE Transactions on Vehicular Technology*, vol. 65, no. 10, pp. 7831–7843. Mar. 2016.

[9] S., Wu, C.-X., Wang, H., Haas, et al. "A Non-Stationary Wideband Channel Model for Massive MIMO Communication Systems," *IEEE Transactions on Wireless Communications*, vol. 14, no. 3, pp. 1434–1446, Mar. 2015.

[10] E. G., Larsson, O., Edfors, F., Tufvesson, et al. "Massive MIMO for Next Generation Wireless Systems," *IEEE Communications Magazine*, vol. 52, no. 2, pp. 186–195, Feb. 2014.

[11] F., Rusek, D., Persson, B. K., Lau, et al. "Scaling Up MIMO: Opportunities and Challenges with Very Large Arrays," *IEEE Signal Processing Magazine*, vol. 30, no. 1, pp. 40–60, Jan. 2013.

[12] K., Zheng, S., Ou, X., Yin, "Massive MIMO Channel Models: A Survey," *International Journal of Antennas and Propagation*, vol. 2014, pp. 1–10, June 2014.

[13] Y., Cai, R. C., de Lamare, B., Champagne, et al. "Adaptive Reduced-Rank Receive Processing Based on Minimum Symbol-Error-Rate Criterion for Large-Scale Multiple-Antenna Systems," *IEEE Transactions on Communications*., vol. 63, no. 11, pp. 4185–4201, Nov. 2015.

[14] X., Zhao, S., Li, Q., Wang, et al. "Channel Measurements, Modeling, Simulation and Validation at 32 GHz in Outdoor Microcells for 5G Radio Systems," *IEEE Access*, , vol. 5, pp. 1062–1072, Jan. 2017.

[15] X., Cheng Y., He, "Geometrical model for massive MIMO systems," *IEEE 85th Vehicular Technology Conference (VTC Spring)* ,pp. 1–6, June 2017.

[16] C.-X., Wang, S., Wu, L., Bai, et al. "Recent Advances and Future Challenges for Massive MIMO Channel Measurements and Models," *Science China Information Sciences*, vol. 59, no. 2, pp. 1–16, Feb. 2016.

[17] J.-q., Chen, Z., Zhang, T., Tang, et al. "A Non-Stationary Channel Model for 5G Massive MIMO Systems," *Frontiers of Inf. Tech. & Electronic Engineering*, vol. 18, no. 12, pp. 2101–2110, Dec. 2017.

[18] Y., Chen, Y., Li, S., Sun, et al. "A twin-multi-ring channel model for Massive MIMO system," *16th International Symposium on Communications and Information Technologies (ISCIT)*, pp. 606–610, Sept. 2016.

[19] J., Yao, H., Ren, Q., Liu, "Massive MIMO channel modeling using map-based ray tracing method," *7th IEEE International Symposium on Microwave, Antenna, Propagation, and EMC Technologies (MAPE)*, pp. 1–5. Oct. 2017.

[20] C. F., López, C.-X., Wang, "Novel 3-D Non-Stationary Wideband Models for Massive MIMO Channels," *IEEE Transactions on Wireless Communications*, vol. 17, no. 5, pp. 2893–2905, May 2018.

[21] S., Wu, C.-X., Wang, M. M., Alwakeel, et al. "A Non-Stationary 3-D Wideband Twin-Cluster Model for 5G Massive MIMO Channels," *IEEE Journal on Selected Areas in Communications*, vol. 32, no. 6, pp. 1207–1218, June 2014.

[22] L., Bai, C.-X.,Wang, S., Wu, et al. "A 3-D wideband multi-confocal ellipsoid model for wireless massive MIMO communication channels with uniform planar antenna array," *IEEE 85th Vehicular Technology Conference (VTC Spring)*, pp. 1–6, June 2017.

[23] S., Wu, C.-X., Wang, M. M., Alwakeel, et al. "A General 3-D Non-Stationary 5G Wireless Channel Model," *IEEE Transactions on Communications*, vol. 66, no. 7, pp. 3065–3078, July 2018.

[24] J., Meinilä, P., Kyösti, T., Jämsä, et al. "WINNER II channel models," *Radio Technologies and Concepts for IMT-Advanced*, pp. 39–92, 2009.

[25] A. A., Saleh, R., Valenzuela, "A Statistical Model for Indoor Multipath Propagation," *IEEE Journal on Selected Areas in Communications*, vol. 5, no. 2, pp. 128–137, Feb. 1987.

[26] J., Chen, X., Yin, S., Wang, "Measurement-based massive MIMO channel modeling in 13–17 GHz for indoor hall scenarios," *IEEE International Conference on Communications (ICC)*, pp. 606–610, May 2016.

[27] R., He, B., Ai, G. L., Stüber, et.al. "Mobility Model-Based Non-Stationary Mobile-to-Mobile Channel Modeling," *IEEE Transactions on Wireless Communications*, vol. 17, no. 7, pp. 4388–4400, July 2018.

[28] S. A., Busari, M. A., Khan, K. M. S., Huq, et al. "Millimetre-wave massive MIMO for cellular vehicle-to-infrastructure communication," *IET Intelligent Transport Systems*, vol. 13, no. 6, pp. 983–990, June 2019.

[29] F., Jiang, C., Li, Z., Gong, et al. "Massive MIMO for Future Vehicular Networks: Compressed-Sensing and Low-Complexity Detection Schemes," *International Wireless Internet Conference*, pp. 53–63, 2017.

[30] D.-T., Phan-Huy, S., Wesemann, J., Björsell, et al. "Adaptive massive MIMO for fast moving connected vehicles: It will work with predictor antennas!" *22nd International ITG Workshop on Smart Antennas*, pp. 1–8, Mar. 2018.

[31] Y., Ma, L. Yang, X., Zheng, "A geometry-based non-stationary MIMO channel model for vehicular communications," China Communications, vol. 15, no. 7, pp. 30–38, July 2018.

[32] Y., Liu, C.-X., Wang, J., Huang, et al. "Novel 3D Non-Stationary mmWave Massive MIMO Channel Models for 5G High-Speed Train Wireless Communications," *IEEE Transactions on Vehicular Technology*, pp. 1–11, Aug. 2018.

[33] H., Jiang, Z., Zhang, J., Dang, et al. "A Novel 3-D Massive MIMO Channel Model for Vehicle-to-Vehicle Communication Environments," *IEEE Transactions on Communications*, vol. 66, no. 1, pp. 79–90, Jan. 2018.

[34] R., He, B., Ai, G. L., Stuber, et al. "A cluster based geometrical model for millimeter wave mobile-to-mobile channels," *IEEE/CIC International Conference on Communications in China (ICCC)*, pp.2848–2863., Oct.2017.

[35] J., Huang, R., Feng, J., Sun, et al. "Multi-frequency millimeter wave massive MIMO channel measurements and analysis," *IEEE Journal on Selected Areas in Communications*, vol. 35, no. 7, p. 1591–1605, July 2017.

[36] B., Ai, K., Guan, R., He, et al. "On indoor millimeter wave massive MIMO channels: Measurement and simulation," *IEEE Journal on Selected Areas in Communications*, vol. 35, no. 7, pp. 1678–1690, July 2017.

[37] J., Li, B., Ai, R., He, et al. "Cluster-Based 3-D Channel Modeling for Massive MIMO in Subway Station Environment," *IEEE Access,* vol. 6, pp. 6257–6272, Dec. 2017.

[38] J., Li, B., Ai, R., He, et al. "Measurement-based characterizations of indoor massive MIMO channels at 2 GHz, 4 GHz, and 6 GHz frequency bands," *IEEE 83rd Vehicular Technology Conference (VTC Spring)*, pp. 1–5, May 2016.

[39] S., Payami, F., Tufvesson, "Channel measurements and analysis for very large array systems at 2.6 GHz," *6th European Conference on Antennas and Propagation (EUCAP)*, pp. 433–437, Mar. 2012.

[40] D., Fei, R., He, B., Ai, et al. "Massive MIMO channel measurements and analysis at 3.33 GHz," *10th International Conference on Communications and Networking in China (ChinaCom)*, pp. 194–198, Aug. 2015.

[41] A. O., Martínez, E., De Carvalho, J. Ø., Nielsen, "Towards very large aperture massive MIMO: A measurement based study," *IEEE Globecom Workshops (GC Wkshps)*, Dec. 2014, pp. 281–286, Dec. 2014.

[42] J., Li, B., Ai, R., He, et al. "The 3D spatial non-stationarity and spherical wavefront in massive MIMO channel measurement," *10th International Conference on Wireless Communications and Signal Processing (WCSP)*, pp. 1–6, Oct. 2018.

[43] J., Chen, X. Yin, X., Cai, et al. "Measurement-Based Massive MIMO Channel Modeling for Outdoor LoS and NLoS Environments," *IEEE Access*, vol. 5, pp. 2126–2140, Jan. 2017.

[44] N., Czink, E., Bonek, L., Hentilä, et al. "Cluster-Based MIMO Channel Model Parameters Extracted from Indoor Time-Variant Measurements," *IEEE Globecom*, pp. 1–5, Nov. 2006.

[45] Y., Li, R. He, S. Lin, et al. "Cluster-based nonstationary channel modeling for vehicle-to-vehicle communications,"

www.SID.ir

IEEE Antennas and Wireless Propagation Letters, vol. 16, p. 1419–1422, Nov. 2016.

[46] M. R., Akdeniz, Y., Liu, M. K., Samimi, et al. "Millimeter wave channel modeling and cellular capacity evaluation," *IEEE Journal on Selected Areas in Communications*, vol. 32, no. 6, pp. 1164–1179, June 2014.

[47] E., Bonek, W., Weichselberger, M., Herdin, et al. "A geometry-based stochastic MIMO channel model for 4G indoor broadband packet access:" Citeseer, 2005.

[48] A., Abdi, M., Kaveh, "A Space-Time Correlation Model for Multielement Antenna Systems in Mobile Fading Channels," *IEEE International Conference on Acoustics, Speech, and Signal Processing. Proceedings*, vol. 20, no. 3, pp. 550–560, Apr. 2002.



Mohammad Mehdi Tamaddondar received his M.Sc. from Sistan and Baluchestan University, Zahedan, Iran in 2013. Since 2014, he is a Ph. D. student at ICT Research Institute (ITRC). His research interests include Wireless Channel Modeling, Massive MIMO Systems and Antenna Designing.



Narges Noori received B.Sc., M.Sc. and Ph.D. degrees (with honors) from the Iran University of Science and Technology (IUST), Tehran, Iran, all in Electrical Engineering, in 1998, 2000 and 2006, respectively. From June 2004 to April 2005, she was with the RF/Microwave and Photonics Group, University of Waterloo, Waterloo, Ontario, Canada as a visiting scholar. In May 2005, she joined ICT Research Institute (ITRC), Tehran, Iran where she is an associate professor. In 2008, she received the best researcher award from the Iran Ministry of ICT. She has several research projects in Radio Communication Group of ITRC. Her research interests include Wireless Communications, Radiowave Propagation and Channel Modeling.

Downloaded from journal.itrc.ac.ir at 11:54 IRDT on Wednesday August 26th 2020

www.SID.ir

Archive of SID

Downloaded from journal.itrc.ac.ir at 11:54 IRDT on Wednesday August 26th 2020

www.SID.ir